Destructive Interference Mediated Topological Transitions in Bilayer Metasurfaces

Bo Wang,* Ruhao Pan,† Lechen Yang, Xu Ji, Haifang Yang, and Junjie Li‡
Beijing National Laboratory for Condensed Matter Physics, Institute of Physics, Chinese Academy of Sciences, 100190 Beijing, China

(Received 17 June 2025; revised 18 November 2025; accepted 5 January 2026; published 26 January 2026)

Optical bound states in the continuum (BICs) are polarization singularities with integer topological charges (ν) in momentum space, whose far-field radiation vanishes in the surrounding radiative states. Here, we study the dynamic evolution of topological charges in symmetry-protected BICs within bilayer metasurfaces. Governed by threefold rotation symmetry (C_3), the topological charges obey $\nu = 3n + 1$ ($n \in \mathbb{Z}$). Theoretically and experimentally, we demonstrate that merely tuning the spacer thickness of the bilayer metasurfaces induces a topological transition from a fundamental charge ($\nu = 1$, $n = 0$) to a high-level charge ($\nu = -2$, $n = -1$) without modifying symmetry. Perturbation theory reveals this transition occurs when the first derivative of the far-field radiation with respect to the Bloch wave number k vanishes at Γ, induced by destructive bilayer interference. This interference simultaneously enhances the quality factors of near-Γ resonances and alters their scaling laws from $\mathcal{O}(k^{-2})$ to $\mathcal{O}(k^{-4})$. Our work introduces a symmetry-preserved mechanism to dynamically control BIC topology.

DOI: 10.1103/646c-jc6s

Introduction—Topological physics has emerged as a pivotal domain in modern physics. Physical systems, including quantum materials [1,2], photonic crystals [3,4], and sonic crystals [5,6], exhibit rich topological properties. Topological states are characterized by topological invariants, such as the Chern number associated with the quantum Hall effect [7]. The discrete jump in topological invariants indicates a topological transition. Bound states in the continuum (BICs) are intensely investigated topological states in photonic systems [8–11]. In metasurfaces, BICs manifest as topological defects or vortex centers in polarization vectors [12–14], carrying conserved quantized charges defined by winding far-field polarization vectors around the BICs [12]. These BICs enable broad applications in lasing [15–18], sensing [19–22], polarization control [23–28], and beam steering [29–31]. Spatial symmetry constrains the topological charges ν of the BICs at the Γ points [12]: $\nu = 3n + 1$ for C_3 symmetry and $\nu = 4n \pm 1$ for C_4 symmetry ($n \in \mathbb{Z}$). High-order topological charges $\nu = -2$ [32–34], allowing deterministic generation of off-Γ BICs [33] and merging BICs [32,35–37], have been demonstrated in metasurfaces with C_6 symmetry, which generally obey $\nu = 6n - 2$. Under certain symmetry, multiple topological charges are allowed. However, nearly all prior works on the symmetry-protected BICs only concern the fundamental topological charges ($n = 0$), high-level charges ($|n| \geq 1$) [38], or transitions from fundamental to high-level charges have remained unrealized.

On the other hand, layer stacking is a powerful way to realize tunable topological states. Bilayer or multilayer Chern insulators have been demonstrated to have high-Chern number states [39–43]. The topological charges of BICs have been manipulated by bilayer interactions [31,44–47] in a symmetry-breaking way. Manipulating BIC topological charges in bilayer metasurfaces (BMs)—particularly transitions from lower-order to high-order while preserving symmetry—remains unexplored.

Here, we theoretically propose and experimentally demonstrate a symmetry-preserved tuning of the at-Γ BICs in BMs from fundamental charges to high-level charges. Our BMs preserve D_{3d} symmetry (including inversion and C_{3v} symmetry), ensuring topological charges obey $\nu = 3n + 1$. To reveal evolutions of the topological charges, we analytically solve all the surrounding resonant states of the BICs by perturbation theory, finding that the far-field radiation of their first-order correction states can vanish when simply tuning the spacer layer thickness due to bilayer destructive interference. When the destructive interference happens, topological transition from $\nu = 1$ ($n = 0$) to $\nu = -2$ ($n = -1$) emerges and the Q factors of all near-Γ resonant states are enhanced, with the scaling laws changing from $\mathcal{O}(k^{-2})$ to $\mathcal{O}(k^{-4})$, where k is the Bloch wave number. The predicted topological transition has been validated with full-wave simulations and angle-resolved spectrum measurements.

Theory—Figure 1(a) shows the structure of our BM. Each layer is composed of a triangular lattice of TiO_2 (refractive index $n_o = 2.46$) nanopillars. All the dimensional parameters for the two layers remain the same, but

*Contact author: wangbo2014@iphy.ac.cn
†Contact author: panruhao@iphy.ac.cn
‡Contact author: jjli@iphy.ac.cn

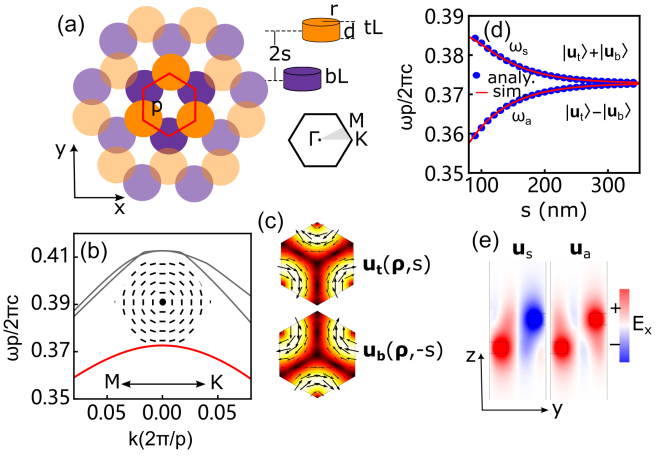

FIG. 1. (a) Schematic of the BM. The parameters are $r = 0.6p$, $d = 0.4p$, and $p = 300$ nm. (b) Band structure for the single-layered structure. Inset: eigenpolarization distribution of the lowest band. (c) Electric-field profiles at the Γ point. (d) Simulated and analytical at-Γ resonant frequencies of the BM. (e) The electric profiles (E_x) in the z-y plane.

the top layer (tL) is shifted along the y axis by p relative to the bottom layer (bL). The tL and bL are vertically separated by $2s$. The refractive index of the surroundings n_s is 1.46. The individual layers are governed by D_{6h} ($C_{6v} \times C_{1h}$) point group. We focus on the lowest TE-like band shown in Fig. 1(b). Its eigenstate at the Γ point belongs to the A irreducible representation of the C_{6v} group, and hence is symmetry-protected at-Γ BIC, carrying polarization singularity with $\nu = +1$ [12] [see the inset of Fig. 1(b)]. The tL and bL alone have the same energy band, but the inversion operator relates their eigenstates at the Γ point [see Fig. 1(c)]. The stack of the two layers breaks the C_6 and up-down mirror symmetry, resulting in the D_{3d} [48] ($C_{3v} \times C_{1i}$) point group. Because of the symmetry breaking, the eigenstates of the two single layers, $|\mathbf{u}_{t,b}\rangle \equiv \mathbf{u}_{t,b}(\boldsymbol{\rho}, z \mp s)$, become mixed, where $(\boldsymbol{\rho}, z)$ is the coordinate. Using group representation theory [49], we find that $|\mathbf{u}_s\rangle \equiv |\mathbf{u}_b\rangle + |\mathbf{u}_t\rangle$ ($|\mathbf{u}_a\rangle \equiv |\mathbf{u}_b\rangle - |\mathbf{u}_t\rangle$) is associated with the A_{2g} (A_{1u}) irreducible representation of the D_{3d} group. Therefore, $|\mathbf{u}_{s,a}\rangle$ are the eigenstates at the Γ points of the BM. Knowing the eigenstates, the corresponding resonant frequencies can be written as [49]

$$\omega_{s,a} = \omega_0^2 \frac{\langle \mathbf{u}_b|(\varepsilon_0+\varepsilon_1)|\mathbf{u}_b\rangle \pm \langle \mathbf{u}_b|(\varepsilon_0+\varepsilon_2)|\mathbf{u}_t\rangle}{\langle \mathbf{u}_b|\varepsilon|\mathbf{u}_b\rangle \pm \langle \mathbf{u}_b|\varepsilon|\mathbf{u}_t\rangle}, \quad (1)$$

where ε_0 is the permittivity for surroundings, $\varepsilon_0 + \varepsilon_{1,2} = n_o^2$, inside TiO_2 nanopillars of the bL and tL, respectively, while in other regions $\varepsilon_{1,2} = 0$, $\varepsilon = \varepsilon_0 + \varepsilon_1 + \varepsilon_2$ and $\langle \mathbf{u}_b|\varepsilon|\mathbf{u}_t\rangle \equiv (1/p^3)\int \tilde{\mathbf{u}}_b(\boldsymbol{\rho}, z+s)\cdot \mathbf{u}_t(\boldsymbol{\rho}, z-s)\varepsilon(\boldsymbol{\rho}, z)\, dz d\boldsymbol{\rho}$; $\tilde{\mathbf{u}}$ is the complex conjugate of $\mathbf{u}$. The analytically calculated $\omega_{s,a}$ according to Eq. (1) are perfectly consistent with the simulated ones by COMSOL Multiphysics software [Fig. 1(d)], indicating that we have found correct eigenstates at the Γ point for the BM. As the electric-field profile of $|\mathbf{u}_{s,a}\rangle$ in Fig. 1(e) indicated, $\mathcal{P}_i|\mathbf{u}_s\rangle = |\mathbf{u}_s\rangle$, while $\mathcal{P}_i|\mathbf{u}_a\rangle = -|\mathbf{u}_a\rangle$, where $\mathcal{P}_i$ is the inversion operator. We hence call photonic bands related to $|\mathbf{u}_s\rangle$ and $|\mathbf{u}_a\rangle$ symmetric band (SB) and antisymmetric band (AB), respectively. Since both $|\mathbf{u}_t\rangle$ and $|\mathbf{u}_b\rangle$ of the single layers are BICs; their linear superpositions, i.e., $|\mathbf{u}_{s,a}\rangle$, are BICs, exhibiting polarization singularity in the momentum spaces with the topological charges generally obeying $\nu = 3n + 1$ ($n \in \mathbb{Z}$) because of the C_3 symmetry. Although $|\mathbf{u}_{s,a}\rangle$ have vanished far-field radiation, the so-called quasi-BICs near the Γ point will radiate. This radiation, contributed from both the tL and bL, is expected to interfere constructively or destructively as s varies. It is the collective behaviors of the whole surrounding quasi-BICs that determine the topological properties of the BICs.

To reveal the interference behavior of the surrounding radiative states around the BICs and the evolutions of the topological charges, we use perturbation theory to directly solve the far-field polarization vectors at a near-Γ Bloch wave vector $\boldsymbol{\alpha} = (2\pi\delta/p)[\cos\theta,\ \sin\theta]^T$, where θ is the angle between $\boldsymbol{\alpha}$ and the x axis, and δ is the perturbation parameter. The perturbation theory can efficiently predict the resonant frequencies $\omega(\delta,\theta)$ and states $|\mathbf{u}(\delta,\theta)\rangle$ at the off-Γ points [50,53], only needing to know the resonant frequency ω_* and state $|\mathbf{u}_*\rangle$ at the Γ point. The spirit of perturbation theory [50] is to expand the resonant states as $|\mathbf{u}(\delta,\theta)\rangle = |\mathbf{u}_*\rangle + \delta|\mathbf{u}_1(\theta)\rangle + \delta^2|\mathbf{u}_2(\theta)\rangle + \cdots$. The first-order correction state $|\mathbf{u}_1(\theta)\rangle$ has a plane-wave asymptotic solution $\sim \mathbf{d}_1^{\pm} e^{\pm i\gamma z}$, where $\gamma = n_s\omega_*/c$, c is the speed of light, and $\mathbf{d}_1^{\pm}$ are the polarization vectors of the upward and downward radiation. We show [49] that the $\mathbf{d}_1^{+}$ can be calculated from

$$\begin{bmatrix} d_{1y}^{+} \\ d_{1x}^{+} \end{bmatrix} = M\kappa_{s,a} \begin{bmatrix} \cos\theta \\ -\sin\theta \end{bmatrix}, \quad (2)$$

where $\kappa_{s,a} = \langle \mathbf{u}_{y*}^{+}|\mathcal{L}_{1x}|\mathbf{u}_{s,a}\rangle = \frac{1}{\sqrt{2}}\langle \mathbf{u}_{y*}^{+}|\mathcal{L}_{1x}|\mathbf{u}_b \pm \mathbf{u}_t\rangle$ and M is a normalization parameter [49], which are solely dependent on the at-Γ BICs. Here, $|\mathbf{u}_{y*}^{+}\rangle$ is the scattering state when a y-polarized plane wave is normally incident onto the top layer, and $\mathcal{L}_{1x}$ is the x component of the first-order perturbation operator. Now, we have obtained a global coupling parameter $\kappa_{s,a}$ that relates the far-field polarization vectors of all the near-Γ states $|\mathbf{u}_{s,a}\rangle + \delta|\mathbf{u}_1(\theta)\rangle$ with the at-Γ states $|\mathbf{u}_{s,a}\rangle$, where θ spans $0 - 2\pi$. In fact, $\kappa_{a,s}$ are the first derivatives of the polarization vectors with respect to the Bloch wave number [54]. According to Eq. (2), $\nu = +1$ ($n = 0$) for the SB and AB if $\kappa_{s,a}$ are nonzero [12]. Note that $\kappa_{s,a}$ are contributed from the tL and bL. Can the addition of the two contributions make $\kappa_{s,a}$ approach zero where destructive interference happens? To answer this question, we derive a detailed form of $\kappa_{s,a}$ to reveal how they vary with s [49],

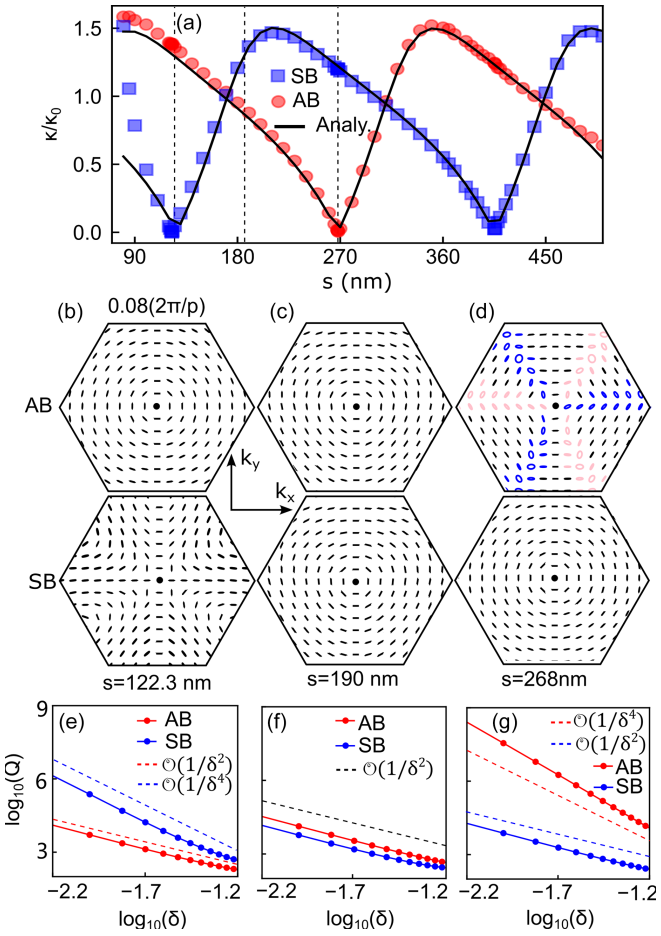

FIG. 2. (a) Simulated and analytical coupling coefficients for the SB and AB. (b)–(d) Polarization vector patterns of the far-field radiation from the SB and AB. The blue and red colors distinguish opposite chirality. (e)–(g) Q factors and their evolution trends with δ. Here, δ changes along the x axis. The dashed lines are guidelines.

$$\kappa_{s,a} = \frac{\kappa_0}{\sqrt{2}} e^{is\gamma} \frac{1 \mp e^{-i(2s\gamma+\varphi)}}{1 \mp \tilde{r}_0 e^{-2is\gamma}}, \tag{3}$$

where κ_0 is the coupling coefficient of the single layer, and $\varphi = \angle(r_0 - t_0)$, r_0 (t_0) is the normal reflection (transmission) coefficient of the single layer. Equation (3) indicates that when $2s\gamma + \varphi = 2N\pi$, $\kappa_s = 0$ and that when $2s\gamma + \varphi = (2N+1)\pi$, $\kappa_a = 0$, where N is an integer. So far, we have demonstrated in theory that far-field radiation of the resonant states near BICs from two separated layers can produce destructive bilayer interference.

We show next that the destructive bilayer interference can boost the Q factors of all near-Γ resonant states and trigger topological transitions of the polarization singularities. Figure 2(a) shows the calculated results of $\kappa_{s,a}$. The squares mark the simulated results according to the definition $\kappa_{s,a} = \langle \mathbf{u}^{+}_{y*} | \mathcal{L}_{1x} | \mathbf{u}_{s,a} \rangle$. The solid curves denote the analytic results from Eq. (3), consistent with the simulation results. Deviations at small s result from the neglect of the interlayer near-field coupling in deriving Eq. (3), which becomes significant when s gets small. Our collective interference theory successfully predicts the destructive interferences at $s = 122.3$ nm for the SB and $s = 268$ nm for the AB.

Figures 2(b)–2(d) show the polarization vector patterns when $s = 122.3$ nm, $s = 190$ nm, and $s = 268$ nm. One can find that when the destructive interference conditions are satisfied, i.e, $s = 122.3$ nm for the SB [Fig. 2(b)] and $s = 268$ nm for the AB [Fig. 2(d)], the ν becomes -2 ($n = -1$). When $\kappa_{a,s}$ deviate far from zero, $\nu = +1$ ($n = 0$) for both the SB and AB [Fig. 2(c)]. These results indicate that the topological charges can transition from $+1$ to -2 by changing s without breaking or boosting symmetry. Although $\nu = -2$ has been demonstrated in B representation of C_{6v} symmetry [32,33], this charge intrinsically belongs to fundamental charge because $n = 0$. In our case, $\nu = -2$ results from that when $\kappa_{s,a} = 0$, the second-order correction states of $\mathbf{u}(\theta)$ will generate far-field polarization vectors $\mathbf{d_2}$, and the C_{3v} group, a subgroup of D_{3d} group, will guarantee that $\mathbf{d_2}$ has $\nu = -2$ ($n = -1$) [49]. Figure S6 [49] shows that three pairs of C points with opposite chirality, exhibiting a total charge of -3, are created and gradually move away from the Γ point as s increases from 122.3 nm. Hence, the total topological charge is conserved. We note that the generation of C-point [23–25,27,28] pairs here requires no symmetry breaking [23,30].

When the wave vector deviates from the Γ point, the Q factor decreases from infinity, typically $\sim\delta^{-2}$ [55]. We show in Figs. 2(e) and 2(g) that when the condition for the destructive interferences is met, the Q factors scale with δ^{-4} near the Γ point of both the SB and AB. When s departs far from the destructive interference conditions, the Q factor $\sim\delta^{-2}$, as shown in Fig. 2(f). Moreover, the near-Γ Q factor becomes much larger when $\kappa_{s,a} = 0$, which results from radiation suppression by destructive interference. The δ^{-4} scaling law originates from the fact that at least $\mathbf{d}_2$ contributes to the radiation leaking when $\mathbf{d}_1^{\pm}$ vanishes. A BIC surrounded by radiative states with Q-factor scaling with δ^{-4} is usually called a "super BIC." Previous schemes to realize super BICs merged a few isolated BICs in the momentum space. Our results present a different way to realize super BICs: merging three pairs of C points. According to Eq. (3), there are infinite s to make $\kappa_{s,a} = 0$, providing more flexibility to realize super BICs. Counterintuitively, the Q-factor enhancement near the Γ point persists even at extremely large separations where near-field coupling vanishes. We verify this by simulating structures with $s \sim 5$–6 μm and $s \sim 99$–100 μm at an incident angle of 2°. As shown in Fig. S7 [49], extremely narrow resonances emerge when $k_{a,s} \approx 0$, demonstrating that the enhancement stems from far-field destructive interference between the radiation channels of the two decoupled layers.

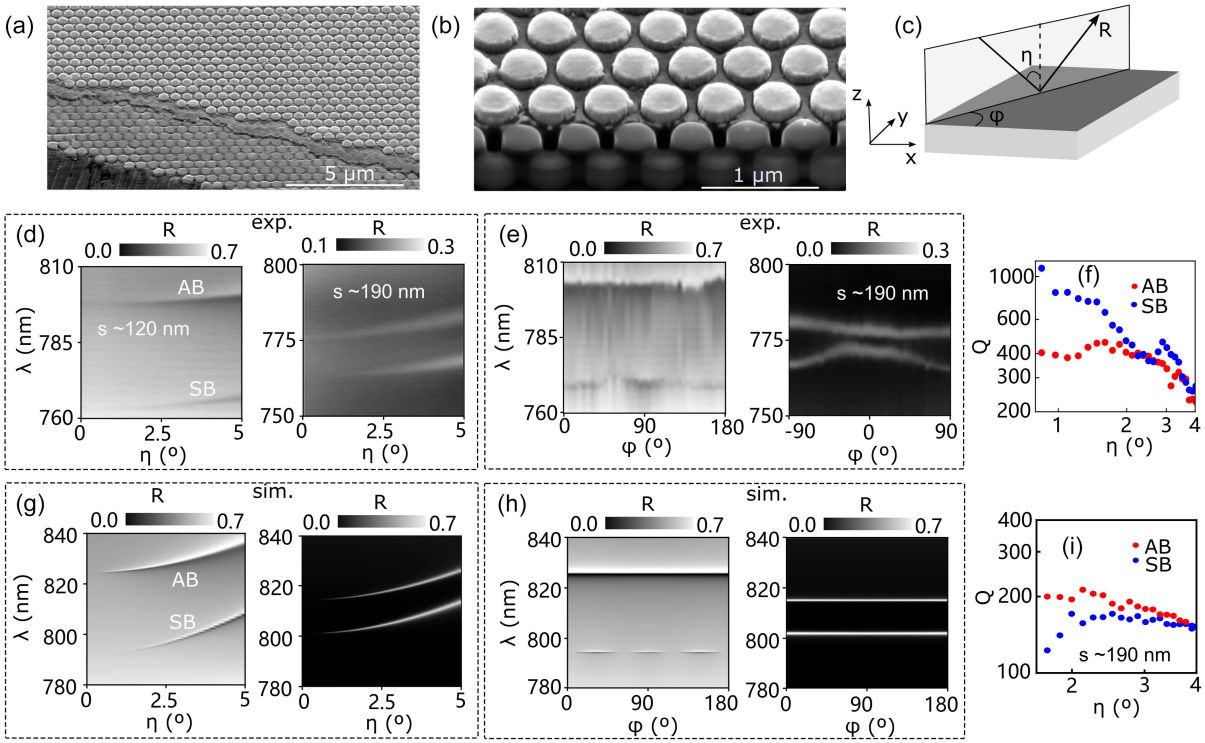

FIG. 3. (a),(b) SEM images of the fabricated BMs. (c) Measurement configuration of the angle-resolved reflection spectra. (d), (g) Experimental and simulated angle-resolved reflection spectra. (e),(h) Experimental and simulated azimuth-angle dependence of the reflection spectra. (f),(i) Extracted Q factors of the BMs with $s = 120$ nm and $s = 190$ nm.

Experiments—We fabricated the designed BMs with their spacer thickness of $s \sim 120$ nm and $s \sim 190$ nm based on the alignment lithography [31]. The detailed fabrication process can be found in our previous paper [56]. The scanning electron microscope (SEM) images shown in Figs. 3(a) and 3(b) confirm the fine alignment and the precise control of the spacing layers. We use a commercial angle-resolved spectrometer [14] (Ideaoptics) to reveal the topological transition of the BICs. Using this spectrometer, one can measure the angle-resolved (η) reflection spectra along each sample azimuthal angle φ, as shown in Fig. 3(c). Figure 3(d) shows the measured spectra when $s \sim 120$ nm and $s \sim 190$ nm. The dispersions of the resonant modes in the SB and AB are clearly presented, which agree with the simulated reflection spectra, as shown in Fig. 3(g). The blue shifts of the measured resonances originate from the dimensional deviation of the fabricated samples. When η approaches 0°, the Fano resonant structures disappear, indicating the existence of BICs. The resonance linewidth of the SB is noticeably narrower than that of the AB when $s \sim 120$ nm, which provides preliminary evidence for destructive interference.

We then rotated the samples and recorded the reflection spectra under the illumination of s-polarized input lights at a fixed η of 4°. The reflectance peak amplitudes scale with $R_{\text{peak}} \propto \cos^2\beta$ [26], where β is the angle between the input light polarization and the major axis of the polarization ellipses. Consider that the sample azimuth angle is φ, the input polarization vector is then $[-\sin\varphi,\ \cos\varphi]^T$. If the topological charge is $+1$ (-2), as shown in Fig. 2(b), the polarization vector is $[-\sin\varphi, \cos\varphi]^T$ ($[-\cos 2\varphi,\ \sin 2\varphi]^T$) and then $R_{\text{peak}} \sim 1$ ($R_{\text{peak}} \sim \sin^2 3\varphi$). Hence, as the samples are rotated by 180°, the reflectance at the resonances remains unchanged when $\nu = +1$ while R_{peak} oscillates by 3 cycles when $\nu = -2$. Figures 3(e) and 3(h) shows the measured and simulated φ-dependent reflection spectra. It can be seen that when $s = 120$ nm, the resonant peaks for the SB oscillate 3 times while those for the AB remain nearly unchanged. When $s = 190$ nm, the resonant peaks for both bands do not oscillate. The experimental results are consistent with the simulated ones. These results indicate that we observed a topological transition of polarization singularities simply by changing the thickness of the BM spacer layer.

Figures 3(f) and 3(i) present the measured Q factors of the resonances, extracted from angle-resolved reflection spectra via a established fitting procedure [57,58] (see Fig. S8 in the Supplemental Material [49]). When $s \sim 190$ nm, the AB and SB modes exhibit comparable Q factors, consistent with theoretical expectations. Notably, at $s \sim 120$ nm—where destructive interference is predicted —the SB mode shows higher Q factors than the AB mode for $\eta < 2°$, reaching a maximum value exceeding 1000 at $\eta \sim 0.85°$. This confirms a measurable Q enhancement attributable to bilayer destructive interference. However,

the scaling behavior of the SB mode deviates substantially from the predicted $\mathcal{O}(\eta^{-4})$ trend.

To understand this discrepancy, we systematically evaluated the influence of various fabrication imperfections—including TiO_2 nanopillar parameters (radius, height, refractive index), spacer thickness, substrate-superstrate asymmetry, and interlayer alignment error—on the Q factors and their angular scaling (see Supplemental Material for details [49]). Our analysis reveals that the $\mathcal{O}(\eta^{-4})$ scaling remains robust against all parameter variations except alignment errors. Although a 5-nm misalignment disrupts the ideal scaling law, the simulated Q factors of the SB mode remain on the order of 10^4–10^5, still surpassing those of the AB mode. This suggests that alignment inaccuracy alone cannot account for the significantly lower Q values obtained in experiments.

We therefore ascribe the significant discrepancy of the measured Q factors to the limited wavelength resolution of our spectrometer. Recent studies on BICs have successfully measured Q factors as high as 10^5–10^6 using tunable lasers with sub-picometer-scale wavelength resolution [59–61]. In contrast, the spectrometer used in our experiments has a resolution of ~0.063 nm, which is insufficient to accurately resolve such high-Q resonances by fitting procedures. The recently demonstrated laser-scanning angle-resolved spectroscopy technique [61] offers a promising path toward resolving the $\mathcal{O}(\eta^{-4})$ scaling in future experiments.

Conclusions—We demonstrate theoretically and experimentally that the topological charges ($\nu = 3n + 1$) of BICs in C_3-symmetric bilayer metasurfaces can be dynamically tuned from fundamental charges ($n = 0$) to high-level charges ($n = -1$) by adjusting the spacer thickness. Theoretically, we establish that this topological transition is triggered by the vanishing first-order derivative of far-field radiation at Γ, induced by bilayer destructive interference. Experimentally, we observe the transition through angle-resolved reflection spectroscopy. Our work provides a symmetry-preserved approach to control BIC topological charges and quasi-BIC Q factors, critical for tunable vortex lasers [62], ultrasensitive sensors [63], and other vortex-based devices. Crucially, we reveal that far-field radiation derivatives—not just the radiation itself—can drive nontrivial topology, offering a new degree of freedom to explore BIC physics. Furthermore, the Q-factor enhancement originates from destructive interference in far-field radiation, and can persist at spacer distances far beyond the range of near-field coupling, enabling greater flexibility in enhancing light-matter interactions.

Acknowledgments—This work was supported by the National Natural Science Foundation of China (Grants No. 12304463, and No. 12074420), and the Chinese Academy of Sciences through the Project for Young Scientists in Basic Research (YSBR-021). This work is technically supported by the IOP-HKUST-Joint Laboratory for Wave Functional Materials Research and the Synergetic Extreme Condition User Facility (SECUF, [64]).

Data availability—The data that support the findings of this article are openly available [65].

[1] A. Bansil, H. Lin, and T. Das, Colloquium: Topological band theory, Rev. Mod. Phys. **88**, 021004 (2016).
[2] H. Luo, P. Yu, G. Li, and K. Yan, Topological quantum materials for energy conversion and storage, Nat. Rev. Phys. **4**, 611 (2022).
[3] L. Lu, J. D. Joannopoulos, and M. Soljačić, Topological photonics, Nat. Photonics **8**, 821 (2014).
[4] T. Ozawa, H. M. Price, A. Amo, N. Goldman, M. Hafezi, L. Lu, M. C. Rechtsman, D. Schuster, J. Simon, O. Zilberberg *et al.*, Topological photonics, Rev. Mod. Phys. **91**, 015006 (2019).
[5] X. Zhang, H.-X. Wang, Z.-K. Lin, Y. Tian, B. Xie, M.-H. Lu, Y.-F. Chen, and J.-H. Jiang, Second-order topology and multidimensional topological transitions in sonic crystals, Nat. Phys. **15**, 582 (2019).
[6] J. Lu, C. Qiu, L. Ye, X. Fan, M. Ke, F. Zhang, and Z. Liu, Observation of topological valley transport of sound in sonic crystals, Nat. Phys. **13**, 369 (2017).
[7] Y. Hatsugai, Chern number and edge states in the integer quantum Hall effect, Phys. Rev. Lett. **71**, 3697 (1993).
[8] C. W. Hsu, B. Zhen, A. D. Stone, J. D. Joannopoulos, and M. Soljačić, Bound states in the continuum, Nat. Rev. Mater. **1**, 16048 (2016).
[9] M. Kang, T. Liu, C. Chan, and M. Xiao, Applications of bound states in the continuum in photonics, Nat. Rev. Phys. **5**, 659 (2023).
[10] W. Liu, W. Liu, L. Shi, and Y. Kivshar, Topological polarization singularities in metaphotonics, Nanophotonics **10**, 1469 (2021).
[11] D. C. Marinica, A. G. Borisov, and S. V. Shabanov, Bound states in the continuum in photonics, Phys. Rev. Lett. **100**, 183902 (2008).
[12] B. Zhen, C. W. Hsu, L. Lu, A. D. Stone, and M. Soljačić, Topological nature of optical bound states in the continuum, Phys. Rev. Lett. **113**, 257401 (2014).
[13] B. Wang, W. Liu, M. Zhao, J. Wang, Y. Zhang, A. Chen, F. Guan, X. Liu, L. Shi, and J. Zi, Generating optical vortex beams by momentum-space polarization vortices centred at bound states in the continuum, Nat. Photonics **14**, 623 (2020).
[14] Y. Zhang, A. Chen, W. Liu, C. W. Hsu, B. Wang, F. Guan, X. Liu, L. Shi, L. Lu, and J. Zi, Observation of polarization vortices in momentum space, Phys. Rev. Lett. **120**, 186103 (2018).
[15] A. Kodigala, T. Lepetit, Q. Gu, B. Bahari, Y. Fainman, and B. Kanté, Lasing action from photonic bound states in continuum, Nature (London) **541**, 196 (2017).
[16] M.-S. Hwang, H.-C. Lee, K.-H. Kim, K.-Y. Jeong, S.-H. Kwon, K. Koshelev, Y. Kivshar, and H.-G. Park, Ultralow-threshold laser using super-bound states in the continuum, Nat. Commun. **12**, 4135 (2021).
[17] Y.-G. Sang, J.-Y. Lu, Y.-H. Ouyang, H.-Y. Luan, J.-H. Wu, J.-Y. Li, and R.-M. Ma, Topological polarization singular

lasing with highly efficient radiation channel, Nat. Commun. **13**, 6485 (2022).
[18] X.-R. Mao, Z.-K. Shao, H.-Y. Luan, S.-L. Wang, and R.-M. Ma, Magic-angle lasers in nanostructured moiré superlattice, Nat. Nanotechnol. **16**, 1099 (2021).
[19] F. Yesilkoy, E. R. Arvelo, Y. Jahani, M. Liu, A. Tittl, V. Cevher, Y. Kivshar, and H. Altug, Ultrasensitive hyperspectral imaging and biodetection enabled by dielectric metasurfaces, Nat. Photonics **13**, 390 (2019).
[20] Y. Jahani, E. R. Arvelo, F. Yesilkoy, K. Koshelev, C. Cianciaruso, M. De Palma, Y. Kivshar, and H. Altug, Imaging-based spectrometer-less optofluidic biosensors based on dielectric metasurfaces for detecting extracellular vesicles, Nat. Commun. **12**, 3246 (2021).
[21] A. Leitis, M. L. Tseng, A. John-Herpin, Y. S. Kivshar, and H. Altug, Wafer-scale functional metasurfaces for mid-infrared photonics and biosensing, Adv. Mater. **33**, 2102232 (2021).
[22] R. E. Jacobsen, A. Krasnok, S. Arslanagic, A. V. Lavrinenko, and A. Alu, Boundary-induced embedded eigenstate in a single resonator for advanced sensing, ACS Photonics **9**, 1936 (2022).
[23] W. Liu, B. Wang, Y. Zhang, J. Wang, M. Zhao, F. Guan, X. Liu, L. Shi, and J. Zi, Circularly polarized states spawning from bound states in the continuum, Phys. Rev. Lett. **123**, 116104 (2019).
[24] Y. Zeng, G. Hu, K. Liu, Z. Tang, and C.-W. Qiu, Dynamics of topological polarization singularity in momentum space, Phys. Rev. Lett. **127**, 176101 (2021).
[25] W. Chen, Z. Wang, M. V. Gorkunov, J. Qin, R. Wang, C. Wang, D. Wu, J. Chu, X. Wang, Y. Kivshar *et al.*, Uncovering maximum chirality in resonant nanostructures, Nano Lett. **24**, 9643 (2024).
[26] C. F. Doiron, I. Brener, and A. Cerjan, Dual-band polarization control with pairwise positioning of polarization singularities in metasurfaces, Phys. Rev. Lett. **133**, 213802 (2024).
[27] Y. Chen, H. Deng, X. Sha, W. Chen, R. Wang, Y.-H. Chen, D. Wu, J. Chu, Y. S. Kivshar, S. Xiao *et al.*, Observation of intrinsic chiral bound states in the continuum, Nature (London) **613**, 474 (2023).
[28] H. Qin, Z. Su, M. Liu, Y. Zeng, M.-C. Tang, M. Li, Y. Shi, W. Huang, C.-W. Qiu, and Q. Song, Arbitrarily polarized bound states in the continuum with twisted photonic crystal slabs, Light Sci. Appl. **12**, 66 (2023).
[29] J. Wang, M. Zhao, W. Liu, F. Guan, X. Liu, L. Shi, C. T. Chan, and J. Zi, Shifting beams at normal incidence via controlling momentum-space geometric phases, Nat. Commun. **12**, 6046 (2021).
[30] J. Wang, L. Shi, and J. Zi, Spin Hall effect of light via momentum-space topological vortices around bound states in the continuum, Phys. Rev. Lett. **129**, 236101 (2022).
[31] D. Gromyko, S. An, S. Gorelik, J. Xu, L. J. Lim, H. Y. L. Lee, F. Tjiptoharsono, Z.-K. Tan, C.-W. Qiu, Z. Dong *et al.*, Unidirectional chiral emission via twisted bi-layer metasurfaces, Nat. Commun. **15**, 9804 (2024).
[32] M. Kang, L. Mao, S. Zhang, M. Xiao, H. Xu, and C. T. Chan, Merging bound states in the continuum by harnessing higher-order topological charges, Light Sci. Appl. **11**, 228 (2022).
[33] T. Yoda and M. Notomi, Generation and annihilation of topologically protected bound states in the continuum and circularly polarized states by symmetry breaking, Phys. Rev. Lett. **125**, 053902 (2020).
[34] Q. Jiang, P. Hu, J. Wang, D. Han, and J. Zi, General bound states in the continuum in momentum space, Phys. Rev. Lett. **131**, 013801 (2023).
[35] M. Kang, S. Zhang, M. Xiao, and H. Xu, Merging bound states in the continuum at off-high symmetry points, Phys. Rev. Lett. **126**, 117402 (2021).
[36] G. Sun, Y. Wang, Y. Li, Z. Cui, W. Chen, and K. Zhang, Tailoring topological nature of merging bound states in the continuum by manipulating structure symmetry of the all-dielectric metasurface, Phys. Rev. B **109**, 035406 (2024).
[37] J. Jin, X. Yin, L. Ni, M. Soljačić, B. Zhen, and C. Peng, Topologically enabled ultrahigh-q guided resonances robust to out-of-plane scattering, Nature (London) **574**, 501 (2019).
[38] High-level topological charges should be distinguished from the high-order topological charges. High-order topological charge of -2 can be realized in systems with C_6 symmetry, but it is a intrinsically fundamental charge because $n = 0$.
[39] Y.-F. Zhao, R. Zhang, R. Mei, L.-J. Zhou, H. Yi, Y.-Q. Zhang, J. Yu, R. Xiao, K. Wang, N. Samarth *et al.*, Tuning the Chern number in quantum anomalous Hall insulators, Nature (London) **588**, 419 (2020).
[40] Y. Sha, J. Zheng, K. Liu, H. Du, K. Watanabe, T. Taniguchi, J. Jia, Z. Shi, R. Zhong, and G. Chen, Observation of a Chern insulator in crystalline ABCA-tetralayer graphene with spin-orbit coupling, Science **384**, 414 (2024).
[41] X. Li, X. Xu, H. Zhou, H. Jia, E. Wang, H. Fu, J.-T. Sun, and S. Meng, Tunable topological states in stacked Chern insulator bilayers, Nano Lett. **23**, 2839 (2023).
[42] S. Mondal and S. Basu, Band-engineered bilayer Haldane model: Evidence of multiple topological phase transitions, Phys. Rev. B **108**, 045307 (2023).
[43] W. Zhu, C. Song, H. Bai, L. Liao, and F. Pan, High Chern number quantum anomalous Hall effect tunable by stacking order in van der Waals topological insulators, Phys. Rev. B **105**, 155122 (2022).
[44] X. Ni, Y. Liu, B. Lou, M. Zhang, E. L. Hu, S. Fan, E. Mazur, and H. Tang, Three-dimensional reconfigurable optical singularities in bilayer photonic crystals, Phys. Rev. Lett. **132**, 073804 (2024).
[45] Z.-P. Zhuang, H.-L. Zeng, X.-D. Chen, X.-T. He, and J.-W. Dong, Topological nature of radiation asymmetry in bilayer metagratings, Phys. Rev. Lett. **132**, 113801 (2024).
[46] M. Kang, M. Xiao, and C. T. Chan, Janus bound states in the continuum with asymmetric topological charges, Phys. Rev. Lett. **134**, 013805 (2025).
[47] K. Y. Lee, K. W. Yoo, S. Cheon, W.-J. Joo, J. W. Yoon, and S. H. Song, Synthetic topological nodal phase in bilayer resonant gratings, Phys. Rev. Lett. **128**, 053002 (2022).
[48] M. S. Dresselhaus, G. Dresselhaus, and A. Jorio, *Group Theory: Application to the Physics of Condensed Matter* (Springer Science & Business Media, New York, 2007).
[49] See Supplemental Material at http://link.aps.org/supplemental/10.1103/646c-jc6s for detailed derivations of Eqs. (1)–(3), the analysis of fabrication errors, and fitting

results of reflection spectra, which includes Refs. [12,32,37,50–52].

[50] N. Zhang and Y. Y. Lu, Perturbation theory for resonant states near a bound state in the continuum, Phys. Rev. Lett. **134**, 013803 (2025).

[51] C. Menzel, C. Rockstuhl, and F. Lederer, Advanced Jones calculus for the classification of periodic metamaterials, Phys. Rev. A **82**, 053811 (2010).

[52] K. Sakoda, Proof of the universality of mode symmetries in creating photonic dirac cones, Opt. Express **20**, 25181 (2012).

[53] T. Weiss, M. Mesch, M. Schäferling, H. Giessen, W. Langbein, and E. A. Muljarov, From dark to bright: First-order perturbation theory with analytical mode normalization for plasmonic nanoantenna arrays applied to refractive index sensing, Phys. Rev. Lett. **116**, 237401 (2016).

[54] Generally, the first derivative of a 2D vector field $[F_x(x,y)F_y(x,y)]$ is a 2×2 matrix. In our case, constrained by symmetry, $\kappa_{a,s}$ are scalars.

[55] K. Koshelev, S. Lepeshov, M. Liu, A. Bogdanov, and Y. Kivshar, Asymmetric metasurfaces with high-q resonances governed by bound states in the continuum, Phys. Rev. Lett. **121**, 193903 (2018).

[56] J. Tan, R. Pan, Y. Xiang, Z. Tang, B. Wang, and J. Li, Unilateral asymmetric radiation in bilayer metasurfaces, Adv. Funct. Mater. **35**, 2501156 (2025).

[57] J.-H. Park, A. Ndao, W. Cai, L. Hsu, A. Kodigala, T. Lepetit, Y.-H. Lo, and B. Kanté, Symmetry-breaking-induced plasmonic exceptional points and nanoscale sensing, Nat. Phys. **16**, 462 (2020).

[58] A. Kodigala, T. Lepetit, and B. Kanté, Engineering resonance dynamics of plasmon hybridized systems, J. Appl. Phys. **117**, 023110 (2015).

[59] Z. Chen, X. Yin, J. Jin, Z. Zheng, Z. Zhang, F. Wang, L. He, B. Zhen, and C. Peng, Observation of miniaturized bound states in the continuum with ultra-high quality factors, Sci. Bull. **67**, 359 (2022).

[60] K. Watanabe, T. Nagao, and M. Iwanaga, Low-contrast bic metasurfaces with quality factors exceeding 100,000, Nano Lett. **25**, 2777 (2025).

[61] J. Fang, R. Chen, D. Sharp, E. M. Renzi, A. Manna, A. Kala, S. A. Mann, K. Yao, C. Munley, H. Rarick *et al.*, Million-q free space meta-optical resonator at near-visible wavelengths, Nat. Commun. **15**, 10341 (2024).

[62] Z. Zhang, X. Qiao, B. Midya, K. Liu, J. Sun, T. Wu, W. Liu, R. Agarwal, J. M. Jornet, S. Longhi *et al.*, Tunable topological charge vortex microlaser, Science **368**, 760 (2020).

[63] M. Cheng, W. Jiang, L. Guo, J. Li, and A. Forbes, Metrology with a twist: Probing and sensing with vortex light, Light Sci. Appl. **14**, 4 (2025).

[64] https://cstr.cn/31123.02.SECUF.

[65] B. Wang, Rcwa codes, comsol models and raw data, 10.6084/m9.figshare.30647513.v1 (2025).